

**Key Points:**

- SST in 2004, 2006, and 2016 broke the previous record of satellite observations in the Yellow and East China Seas
- The record-breaking SSTs in these 3 years were mainly attributed to enhanced solar radiation and weakened wind
- Enhanced solar radiation and weakened wind were associated with a high-pressure system splitting from the Pacific subtropical high

**Correspondence to:**

F. Chai,  
fchai@sio.org.cn

**Citation:**

Yan, Y., Chai, F., Xue, H., & Wang, G. (2020). Record-breaking sea surface temperatures in the Yellow and East China Seas. *Journal of Geophysical Research: Oceans*, 125, e2019JC015883. <https://doi.org/10.1029/2019JC015883>

Received 24 NOV 2019

Accepted 20 JUL 2020

Accepted article online 24 JUL 2020

## Record-Breaking Sea Surface Temperatures in the Yellow and East China Seas

**Yunwei Yan<sup>1,2</sup> , Fei Chai<sup>1,3</sup> , Huijie Xue<sup>3,4</sup> , and Guihua Wang<sup>2,5</sup> **

<sup>1</sup>State Key Laboratory of Satellite Ocean Environment Dynamics, Second Institute of Oceanography, Ministry of Natural Resources, Hangzhou, China, <sup>2</sup>Southern Marine Science and Engineering Guangdong Laboratory (Zhuhai), Zhuhai, China, <sup>3</sup>School of Marine Sciences, University of Maine, Orono, ME, USA, <sup>4</sup>State Key Laboratory of Tropical Oceanography, South China Sea Institute of Oceanology, Chinese Academy of Sciences, Guangzhou, China, <sup>5</sup>Department of Atmospheric and Oceanic Sciences and Institute of Atmospheric Sciences, Fudan University, Shanghai, China

**Abstract** Satellite observations of sea surface temperature (SST) show that SST in 2004, 2006, and 2016 broke the previous record in the Yellow and East China Seas (YECS). The underlying cause of the record-breaking SSTs in the YECS is still under debate. Our analysis results demonstrate that enhanced solar radiation and weakened wind, due to a high-pressure system over the YECS splitting from the western Pacific subtropical high, were mainly responsible for the record-breaking SSTs in these 3 years. The enhanced solar radiation and weakened wind both depressed oceanic turbulent mixing, and more heat was concentrated in a shallower mixed layer, inducing an anomalous SST rise and resulting in the record-breaking SSTs.

### 1. Introduction

Extreme sea surface temperature (SST) events frequently occur in recent years (Lima & Wethey, 2012; Mann et al., 2016, 2017; Oliver et al., 2018). For example, three consecutive record-breaking global mean SSTs in 2014–2016 occurred for the first time since the nineteenth century (Mann et al., 2017). These extreme SST events have significant impacts on marine ecosystems (Smale et al., 2019).

The Yellow and East China Seas (YECS) are the marginal seas east of China (Figure 1a). The climatological monthly mean SST in the YECS reaches the maximum (minimum) in August (February) (Bao & Ren, 2014). The YECS has sustained robust decadal warming in recent decades (Cai et al., 2017; Oey et al., 2013; Wu et al., 2017). The warming was accompanied by more frequent cross-shelf current and vigorous spreading of heat from the Kuroshio (Cai et al., 2017; Oey et al., 2013).

In August 2016, an anomalous warming with the maximum value greater than 2°C occurred in the YECS (Figure 1a; Tan & Cai, 2018). The strong warming resulted in the YECS SST in 2016 breaking the historical record of satellite observations (Figure 1b). Up to now, the cause of the record-breaking SST (the strong warming) in 2016 is still under debate. Tan and Cai (2018) considered increased net heat flux and enhanced warm advection as the main causes of the extreme SST event, while Moon et al. (2019) suggested that increased Changjiang diluted water formed a shallower mixed layer (ML) by producing salt stratification above the top of the thermocline, restricting heat exchanges at the base of the ML and leading to the significant warming. The mechanism producing the record-breaking SST in the YECS needs to be further studied.

In addition to August 2016, an anomalous warming occurred in August 2004 and 2006 as well (Figure 1a), which resulted in the YECS SST in 2004 and 2006 breaking the satellite record back then (Figure 1b). Here we first investigate the record-breaking SSTs in these 3 years using remote sensing SST from the infrared and microwave radiometers and then examine their formation causes based on an ocean model outputs and a suite of atmospheric reanalysis.

### 2. Data and Method

#### 2.1. Remote Sensing SST

To examine the record-breaking SSTs in the YECS, the 1/4° daily Optimum Interpolation SST (OISST) produced by National Oceanic and Atmospheric Administration (NOAA), which combines observations from Advanced Very High Resolution Radiometer (AVHRR), ships, and buoys, is used here (hereafter AVHRR

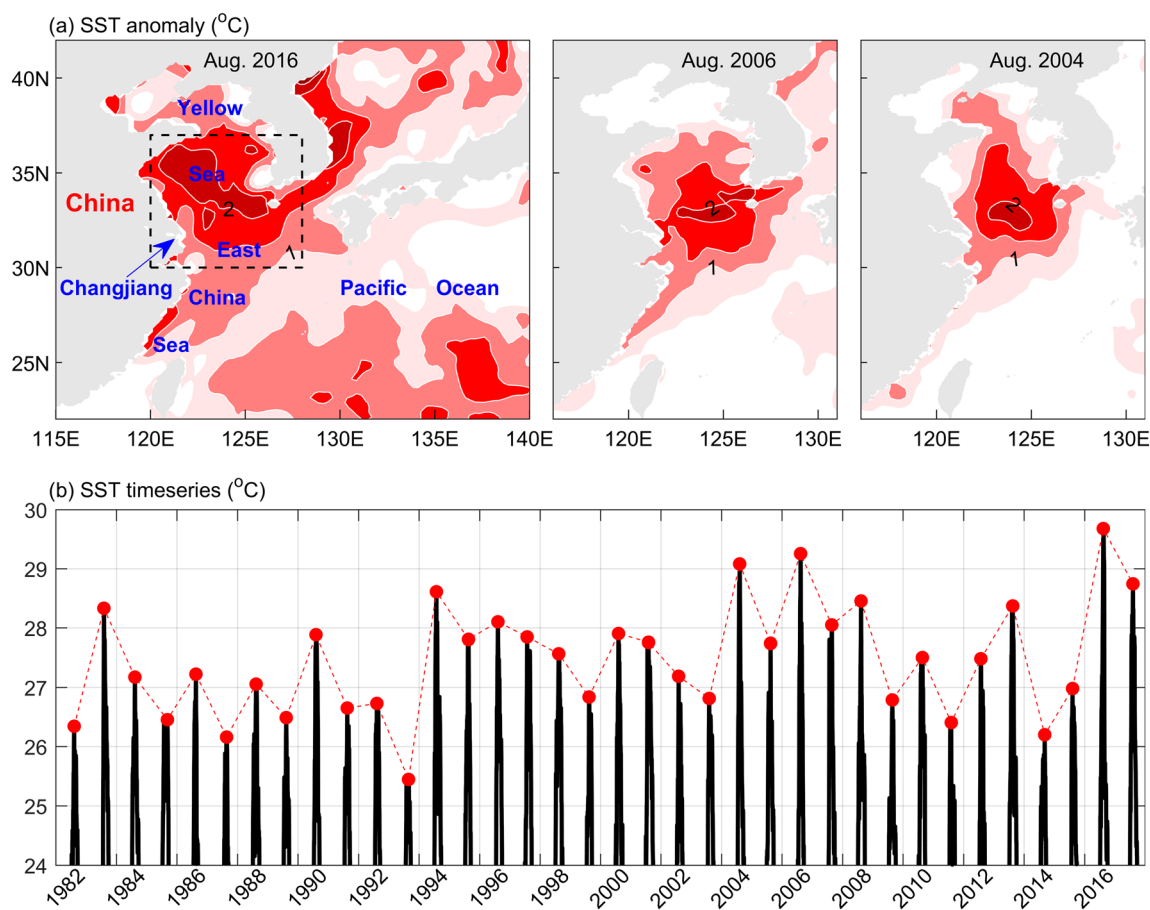


**Figure 1.** (a) Sea surface temperature (SST) anomaly ( $^{\circ}\text{C}$ ) in August 2016, 2006, and 2004 from AVHRR OISST. (b) SST time series ( $^{\circ}\text{C}$ ) in the Yellow and East China Seas (YECS, black dashed box in a,  $120^{\circ}\text{E}$ – $128^{\circ}\text{E}$ ,  $30^{\circ}\text{N}$ – $37^{\circ}\text{N}$ ) from 1982 to 2017. The red dots denote the annual maximum SSTs.

OISST; Banzon et al., 2016; Reynolds et al., 2007). AVHRR has the longest record (from late 1981 to the present) of SST measurements from a single sensor design. Besides, the  $1/4^{\circ}$  daily OISST (from 1998 to the present) combining the microwave radiometer data created by scientists at Remote Sensing Systems (RSS) is also used (hereafter MR OISST). Microwave radiometer can see through clouds and measure SST in most weather conditions (except heavy rain).

## 2.2. OFES Outputs

The Ocean general circulation model For the Earth Simulator (OFES) is a global model, which has a horizontal resolution of  $1/10^{\circ}$  and a vertical resolution of 5 m at the surface (Sasaki et al., 2008). The OFES is driven by daily wind stress, daily surface heat fluxes calculated by the bulk formula of Rosati and Miyakoda (1988), and daily surface freshwater flux. In the calculation of the bulk formula, the model simulated SST is adopted. In addition, river runoff is implicitly included by restoring surface salinity to the climatological monthly mean value of the World Ocean Atlas (WOA) 1998 with the timescale of 6 days. The model is integrated from 1950 after the 50-year climatological spin-up integration (Masumoto et al., 2004), and the snapshot outputs, including sea surface height, temperature, salinity, horizontal and vertical currents, surface wind stress, net surface heat flux, surface freshwater flux and so on, are stored every 3 days.

A comparison of climatological monthly mean temperature and salinity between the OFES and WOA 2013 is conducted in the YECS. The OFES simulated vertical structures of temperature and salinity, including the mixed layer depth (MLD), agree with the WOA 2013 quite well (Figure 2). In addition, the horizontal

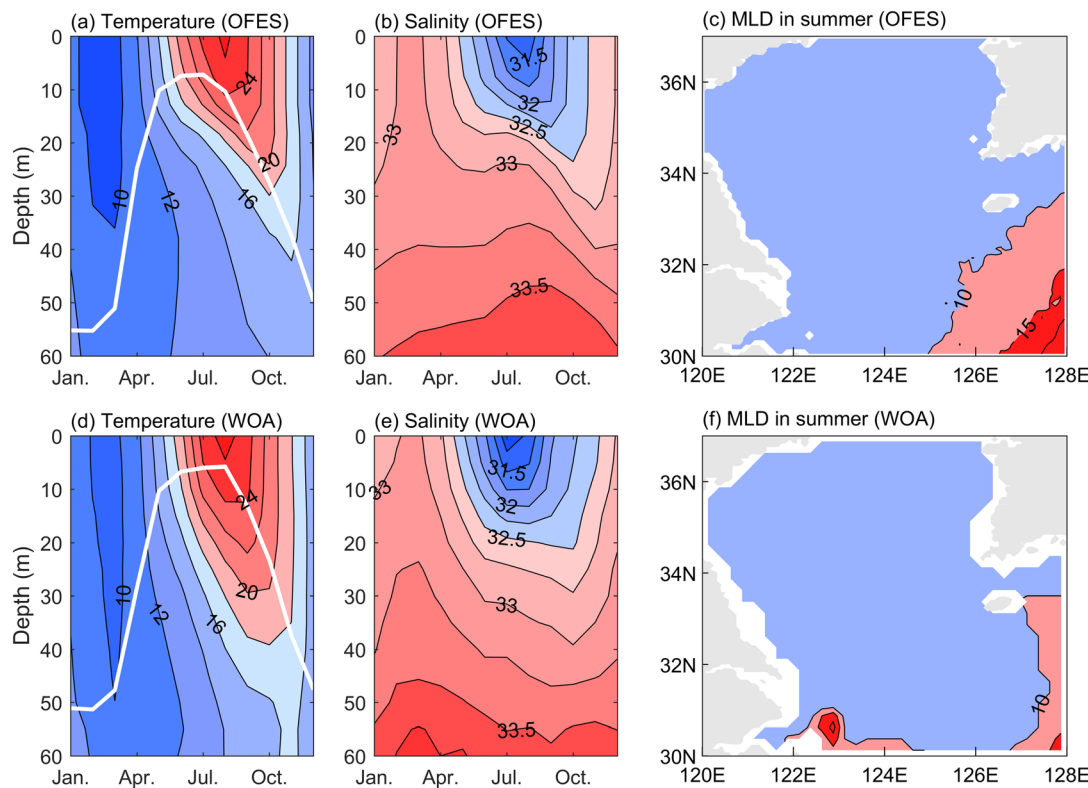


**Figure 2.** Climatological monthly mean temperature ( $^{\circ}\text{C}$ ) (a, d) and salinity (PSU) (b, e) averaged in the YECS and summer mixed layer depth (MLD, m) (c, f) in the YECS from the OFES and WOA 2013. White curves in (a) and (d) denote the MLD.

distributions of the MLD during summer from the OFES and WOA 2013 resemble each other. These results demonstrate that the OFES is capable of reproducing the seasonal evolution and dynamics of mixed layer in the YECS.

### 2.3. Atmospheric Reanalysis

Daily surface heat fluxes and/or wind fields from the NCEP (the National Centers for Environmental Prediction) reanalysis 1 (Kalnay et al., 1996) and reanalysis 2 (Kanamitsu et al., 2002), CFS (Climate Forecast System; Saha et al., 2010, 2014), and multisatellite blended sea winds (Zhang et al., 2006) are used to compare with those from the OFES outputs. Daily geopotential height at 500 mb is downloaded from the CFS.

### 2.4. Other Observations

Daily precipitation and cloud fraction were observed by the Tropical Rainfall Measuring Mission's (TRMM) Microwave Imager (TMI) and the Moderate Resolution Imaging Spectroradiometer (MODIS) on the Aqua satellite, respectively.

### 2.5. MLT Equation

The ML temperature (MLT) equation can be written as (Moisan & Niiler, 1998)

$$\frac{\partial T_m}{\partial t} = \frac{Q - q_d}{\rho C_p h_m} - \vec{V}_m \cdot \nabla T_m - \frac{w_{ent}(T_m - T_d)}{h_m}$$

where  $T_m$  is the MLT,  $Q$  is the net surface heat flux,  $q_d$  is the downward radiative heat flux at the bottom of the ML,  $\rho$  and  $C_p$  are the reference density and specific heat of seawater,  $h_m$  is the MLD,  $\vec{V}_m$  is the horizontal velocity vertically averaged in the ML,  $w_{ent}$  is the entrainment velocity across the bottom of the

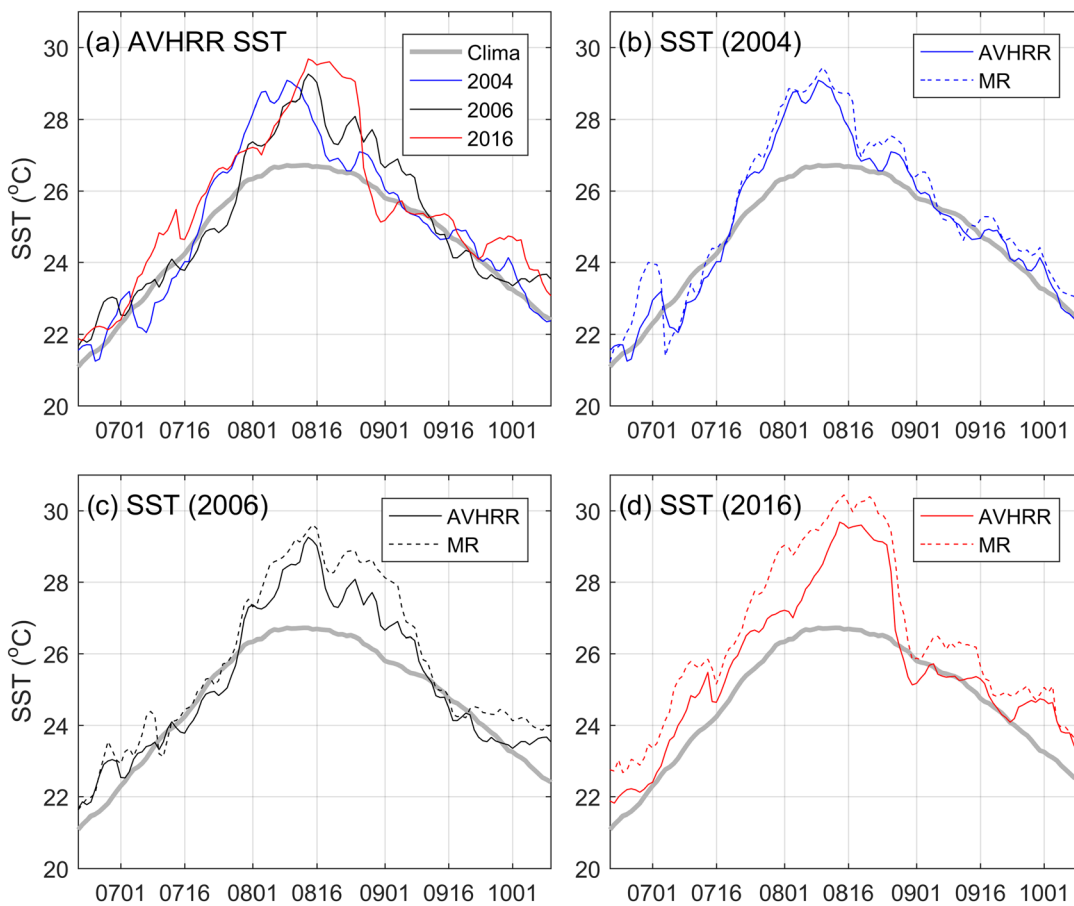


**Figure 3.** (a) SST ( $^{\circ}$ C) in the summer of 2004, 2006, and 2016 and the SST climatology in the YECS from AVHRR OISST. (b–d) SST ( $^{\circ}$ C) in the summer of 2004, 2006, and 2016 from AVHRR and MR OISST.

ML, and  $T_d$  is the temperature just below the ML. The four terms from left to right are referred to as the ML tendency term, the surface heat flux term, the horizontal advection term, and the vertical entrainment term in the following.

To uncover the causes of the record-breaking SSTs in the YECS, all the terms in the MLT equation are calculated from the OFES outputs. In the calculation, the MLD is defined as the depth at which the temperature has decreased by  $0.5^{\circ}$ C relative to the SST (Kelly & Qiu, 1995; Price et al., 1986). Following Qu (2001), the entrainment velocity is calculated as

$$w_{ent} = \begin{cases} \frac{\partial h_m}{\partial t} + w_d + \vec{V}_d \cdot \nabla h_m, & \frac{\partial h_m}{\partial t} + w_d + \vec{V}_d \cdot \nabla h_m > 0 \\ 0, & \frac{\partial h_m}{\partial t} + w_d + \vec{V}_d \cdot \nabla h_m \leq 0 \end{cases}$$

where  $\vec{V}_d$  and  $w_d$  are the horizontal and vertical velocities at the bottom of the ML. Following Lee et al. (2004), the horizontal advection term for the YECS (black dashed box in Figure 1 for the control volume) is calculated as the advection of the boundary temperature ( $T$ ) relative to the spatially averaged temperature of the domain ( $T_d$ ) by inflows normal to the boundaries

$$\iint_{Western} u(T - T_d) dy dz / V_D + \iint_{Eastern} -u(T - T_d) dy dz / V_D + \iint_{Southern} v(T - T_d) dx dz / V_D + \iint_{Northern} -v(T - T_d) dx dz / V_D$$

here  $V_D$  is the volume and  $u$  and  $v$  are eastward and northward velocities, respectively.

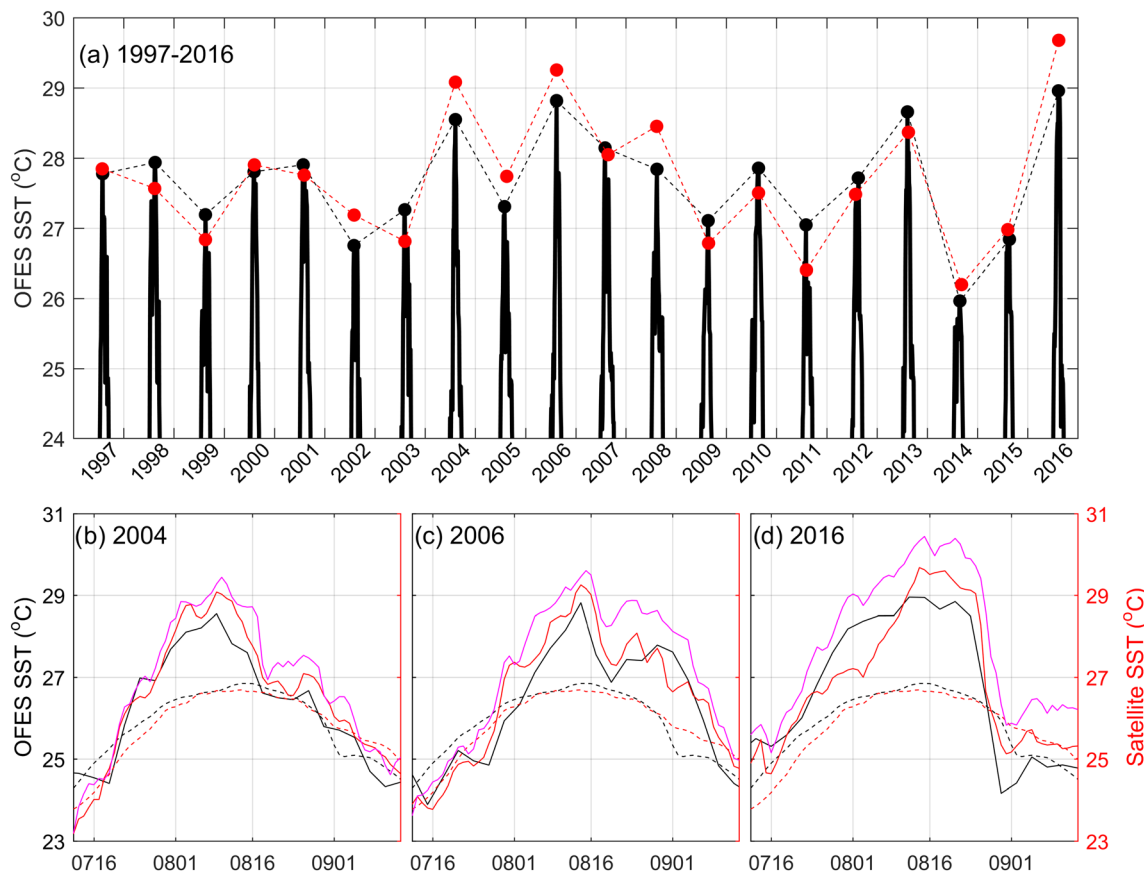
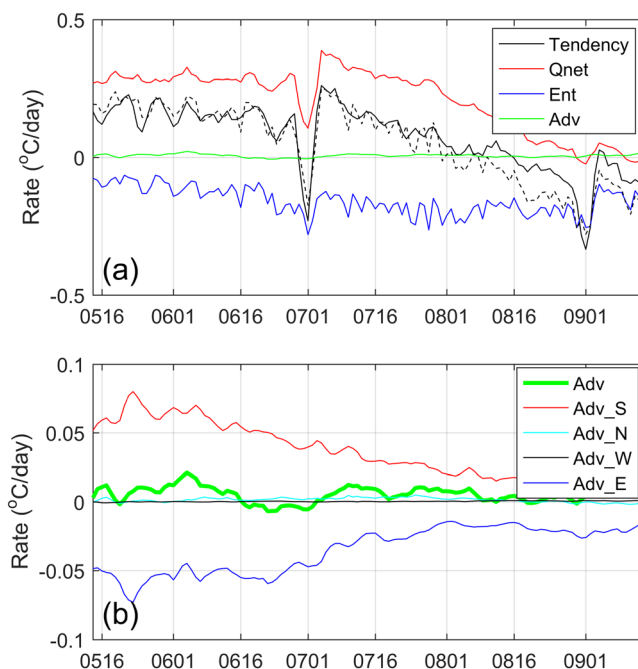


**Figure 4.** (a) SST time series ( $^{\circ}$ C) in the YECS from the OFES outputs. The black and red dots denote the annual maximum SSTs from the OFES outputs and AVHRR OISST, respectively. (b–d) YECS SST ( $^{\circ}$ C) in 2004, 2006, and 2016 from the OFES outputs (solid black lines) and AVHRR (solid red lines) and MR (solid magenta lines) OISST. The dashed black (red) lines denote the SST climatology from the OFES outputs (AVHRR OISST).

### 3. Record-Breaking SSTs in 2004, 2006, and 2016

Figure 3a shows the SST in the summer of 2004, 2006, and 2016 and the SST climatology in the YECS from AVHRR OISST. The climatological YECS SST rises rapidly from  $22.30^{\circ}$ C to  $26.31^{\circ}$ C in July. In the first half of August, the rate of the warming decreases dramatically. The climatological SST reaches the maximum on 13 August with the value of  $26.72^{\circ}$ C. By contrast, the SST in 2004, 2006, and 2016 rose faster in the second half of July and/or the first half of August. It seems the anomalous SST rise resulted in the record-breaking SSTs in these 3 years. The record-breaking SSTs were  $29.08^{\circ}$ C,  $29.25^{\circ}$ C, and  $29.68^{\circ}$ C in these 3 years. We also check the SST in these 3 years from MR OISST. An anomalous SST rise occurred in the second half of July and/or the first half of August, which was consistent with that from AVHRR OISST (Figures 3b–3d). The record-breaking SSTs from MR OISST were  $0.36^{\circ}$ C,  $0.35^{\circ}$ C, and  $0.76^{\circ}$ C greater than those from AVHRR OISST in these 3 years.

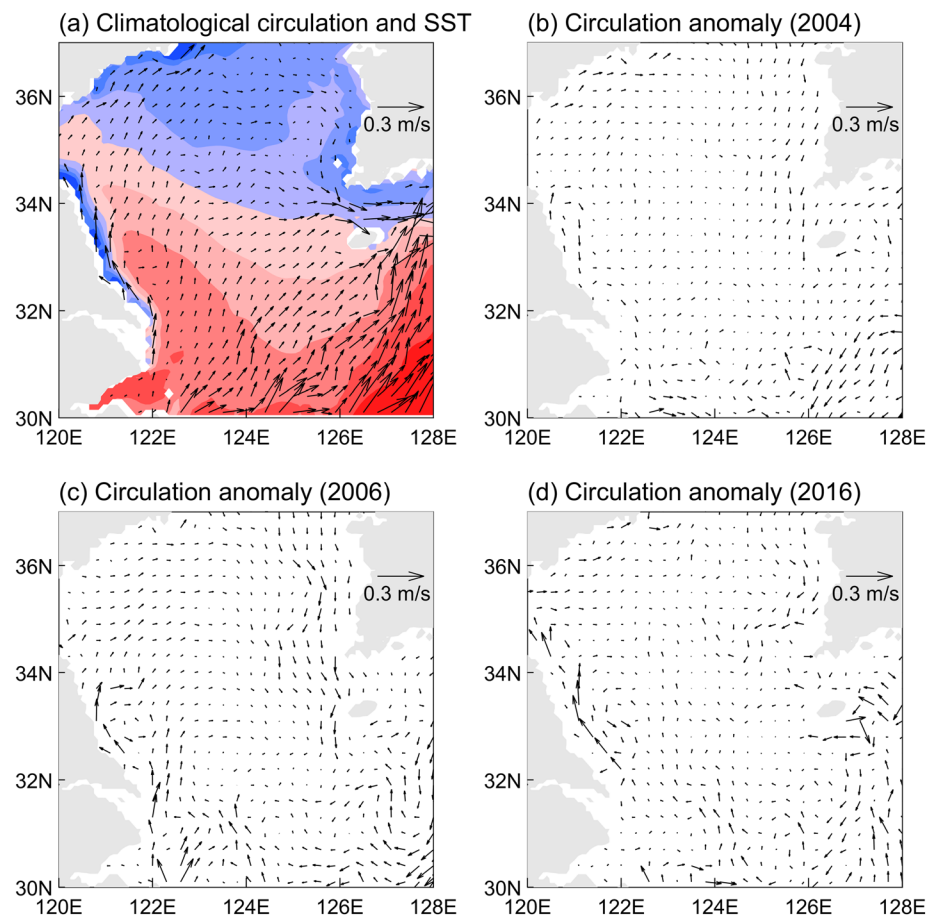
To uncover the underlying cause of the record-breaking SSTs (the anomalous SST rise) in 2004, 2006, and 2016, the OFES outputs are used here. It is worth noting that SST is not assimilated or relaxed in the OFES (Sasaki et al., 2008). Figure 4a shows the OFES simulated SST in the YECS from 1997 to 2016. The annual maximum SST from the OFES outputs exhibited a similar variation with that from AVHRR OISST: The correlation coefficient between them from 1997 to 2016 is 0.91. Especially, the OFES is able to reproduce the record-breaking SSTs in 2004, 2006, and 2016, although the simulated record-breaking SSTs were  $0.53^{\circ}$ C,  $0.44^{\circ}$ C, and  $0.72^{\circ}$ C lower than the observed ones in these 3 years. Zooming in on SST in these 3 years, the anomalous rise in the second half of July and/or the first half of August is also simulated quite well in the OFES (Figures 4b–4d).



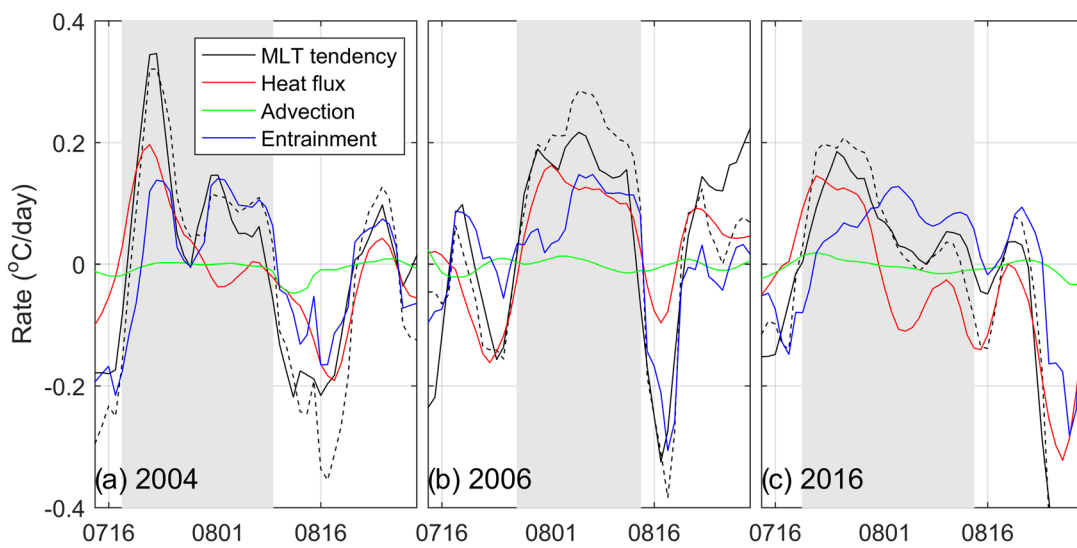
**Figure 5.** (a) All the terms in the MLT equation over the YECS calculated from the OFES outputs: the MLT tendency term (solid black line), the surface heat flux term (red line), the horizontal advection term (green line), and the vertical entrainment term (blue line). The dashed black line denotes the sum of the surface heat flux term, the horizontal advection term, and the vertical entrainment term. (b) Horizontal advection term (green line) and the contributions from the southern (red line), northern (cyan line), western (black line), and eastern (black line) boundaries.

Figure 5a shows the climatologies of all the terms in the MLT equation for the YECS. It is clear that the contribution of ocean horizontal advection is much less than that of surface heat flux and vertical entrainment in summer. During summer, the prevailing surface current direction is northeastward in the YECS (Figure 6a), due to prevailing southeasterly wind (Moon et al., 2009; Xia et al., 2006). Warmer water is advected into the YECS at the southern boundary by northward velocity and out of the YECS at the eastern boundary by eastward velocity (Figure 6a). The advection of warmer water into the YECS from the southern boundary is almost balanced by that out of the YECS from the eastern boundary (Figure 5b). Thus, the horizontal advection term makes little net contribution for the YECS. This means that the MLT variability in the YECS during summer is mainly determined by 1-D vertical processes controlled by atmospheric forcing. The result is consistent with the findings of Kim et al. (2018) based on mooring observations: Atmospheric forcing, including surface heat flux and wind, plays a critical role in determining the MLD variability in the central Yellow Sea, where ocean current is relatively weak.

Figure 7 shows the anomalies of all the terms in the MLT equation in 2004, 2006, and 2016 relative to the daily climatology. The positive anomaly of the MLT tendency term means that the MLT rises faster or drops slower than the climatology. The gray shadings indicate the periods of positive anomaly of the MLT tendency term, which correspond to the aforementioned anomalous SST rise in the second half of July and/or the first half of August. During the record warming periods in these 3 years, the anomaly of the horizontal advection term was almost zero. This was because there was not robust anomalous inflow/outflow through the boundaries into/out of the YECS (Figures 6b–6d). The anomaly of the inflow/outflow velocity averaged along each boundary was smaller than 3 cm/s. Hence, the anomaly of the horizontal advection term could be ignored. The positive anomaly of the MLT tendency term was induced by the anomalies of the surface heat flux term and the vertical entrainment term, meaning that the anomalous SST rise (the record-breaking SST) was produced by one-dimensional vertical processes controlled by atmospheric forcing.



**Figure 6.** (a) Summer climatological surface circulation (arrows) and temperature (color) in the YECS and (b-d) surface circulation anomalies during the warming periods in 2004, 2006, and 2016.



**Figure 7.** Anomalies of all the terms in the MLT equation in 2004, 2006, and 2016 relative to the daily climatology calculated from the OFES outputs: anomalies of the MLT tendency term (solid black lines), the surface heat flux term (red lines), the horizontal advection term (green lines), and the vertical entrainment term (blue lines). The dashed black lines denote the sum of the anomalies of the surface heat flux term, the horizontal advection term, and the vertical entrainment term. The gray shadings indicate the periods of positive anomaly of the MLT tendency term.

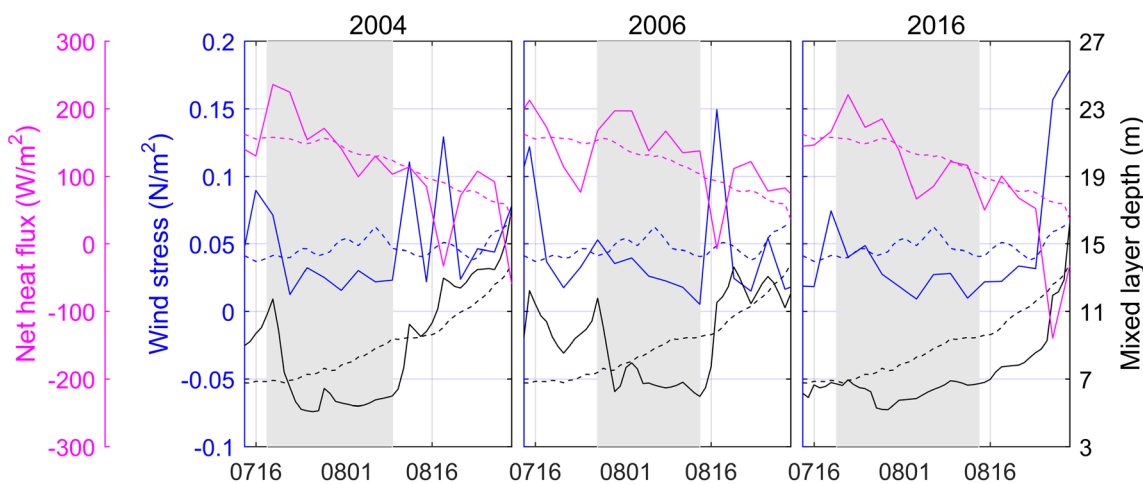


**Figure 8.** Net surface heat flux ( $\text{W/m}^2$ , solid magenta lines), surface wind stress magnitude ( $\text{N/m}^2$ , solid blue lines), and mixed layer depth (m, solid black lines) in 2004, 2006, and 2016 from the OFES outputs. The dashed lines denote the climatology.

At the initial/early stage of the period of the anomalous SST rise, net surface heat flux increased in all these three cases (a positive anomaly, Figure 8), causing a positive anomaly in the surface heat flux term and resulting in the anomalous SST rise (Figure 7). Meanwhile, the magnitude of surface wind stress decreased from a positive anomaly to a negative anomaly (Figure 8). The negative wind stress magnitude anomaly persisted until the end of this period, suppressing oceanic turbulent mixing (a negative MLD anomaly). The reduced turbulent mixing induced a positive anomaly in the vertical entrainment term and led to further anomalous SST rise (Figure 7). Note that the increased net surface heat flux persisted during the whole period in 2006 (Figure 8), which always contributed to the anomalous SST rise (Figure 7).

The results of the MTL equation suggest that the net surface heat flux and surface wind stress were the two most important factors for the record-breaking SSTs in the YECS. The two variables from the OFES outputs are compared with those from atmospheric reanalysis products and satellite data set, including the NCEP reanalyses 1 and 2, CFS, and multisatellite blended sea winds. Because all the four data sets provide surface wind speed, the surface wind stress is replaced with the surface wind speed for comparison here. The surface wind speed from these three reanalysis products and the satellite data showed similar variations during the period of the anomalous SST rise. Surface wind speed initially decreased from a positive anomaly to a negative anomaly, and then the negative anomaly persisted to the end of this period (Figure 9). The behavior of the wind field from the four data sets was consistent with that from the OFES outputs. However, the net surface heat flux from these three reanalysis products showed a positive anomaly during the whole period in all these 3 years, which was different from the OFES outputs. We chose to believe in these three reanalysis products, because the upward surface heat flux in the OFES was calculated from the simulated SST rather than the observed one (Rosati & Miyakoda, 1988). The underestimate of the net surface heat flux in the OFES is a possible reason for the lower record-breaking SSTs in the simulation, as shown in Figure 4.

The net surface heat flux consists of four components: solar radiation, longwave radiation, and latent and sensible heat fluxes. To find out the cause for the increased net surface heat flux, the four components in these 3 years from the CFS are shown in Figure 10. It is clear that the increased solar insolation made a major contribution to the increased net surface heat flux and the reduced latent surface heat flux to the atmosphere from the ocean surface, corresponding to the decreased surface wind speed, played a minor role. The NCEP reanalyses 1 and 2 showed similar results (Figures are not shown).

From above, the record-breaking SSTs in the YECS were mainly attributed to the weakened wind and enhanced solar radiation at the sea surface. The weakened surface wind reduced wind stirring. Moreover, the enhanced solar radiation along with the reduced latent heat flux to the atmosphere from the ocean surface due to the decreased wind speed, hence an increase in the net downward heat flux, enhanced ocean

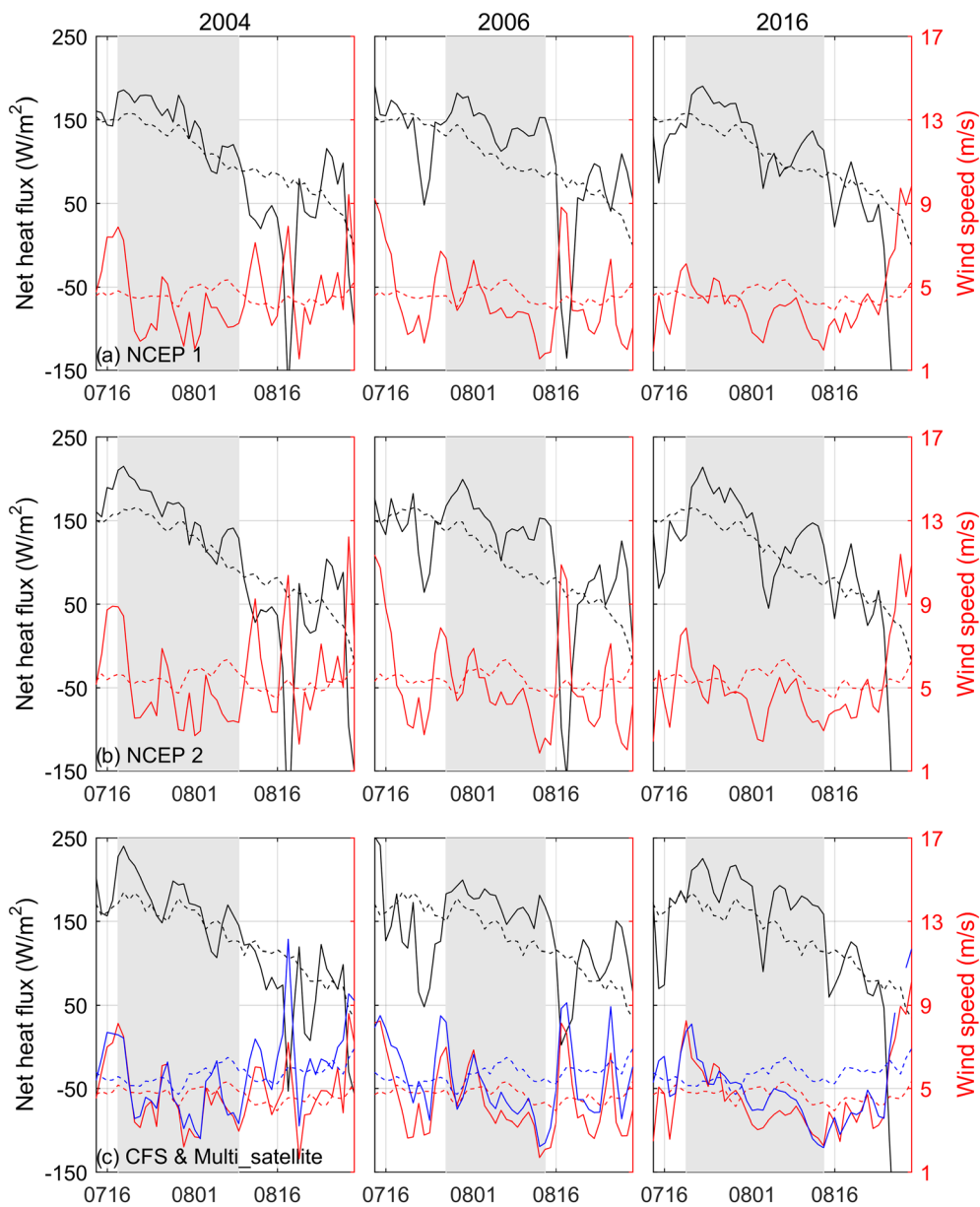


**Figure 9.** Net surface heat flux ( $\text{W/m}^2$ , solid black lines) and surface wind speed (m/s, solid red lines) in 2004, 2006, and 2016 from the NCEP reanalyses 1 (a) and 2 (b) and CFS (c). The solid blue lines in (c) denote surface wind speed from the multisatellite blended sea winds. The dashed lines denote the climatology.

stratification. Both reduced wind stirring and enhanced stratification suppressed oceanic turbulent mixing, and more heat was concentrated in a shallower ML, resulting in the anomalous SST rise and therefore the record-breaking SSTs.

The wind field and solar radiation anomalies during the period of the anomalous SST rise showed an anticyclonic wind anomaly with a positive solar insolation anomaly located over the YECS (Figures 11a–11c). Those anomalies were accompanied by a high-pressure anomaly over the YECS (Figures 11d–11f). The local high-pressure system was split from the western Pacific subtropical high, which then moved westward (not shown). Under the high-pressure condition, there was usually a descending motion over the YECS, with calm or weak wind at the sea surface. Moreover, the descending motion increased atmospheric stability, suppressed cloud formation, and enhanced solar radiation at the sea surface (Figures 11a–11c). The weakened wind and enhanced solar radiation caused the record-breaking SSTs in these 3 years.

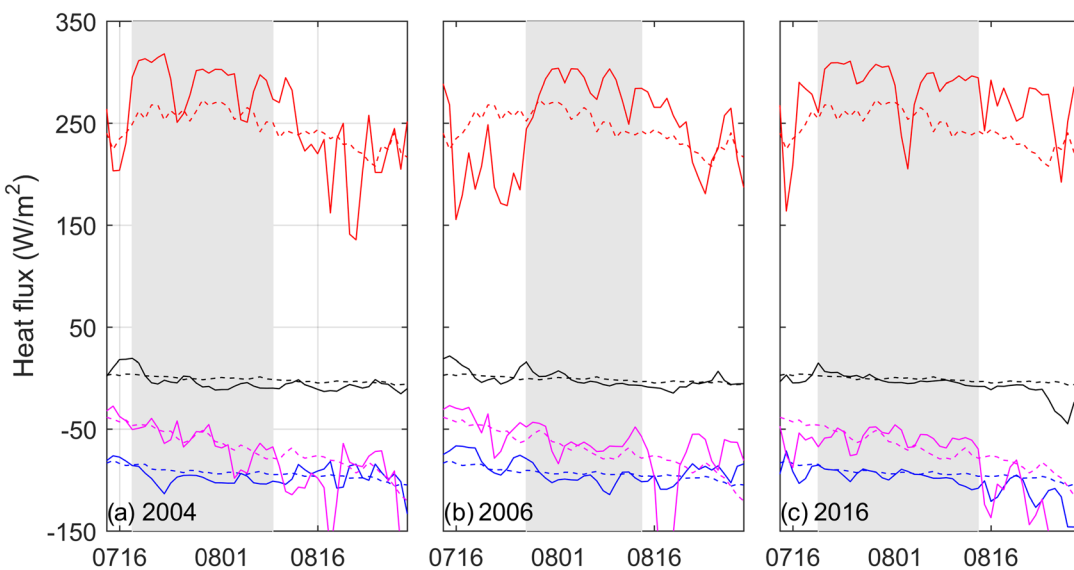


**Figure 10.** Solar radiation (solid red lines), longwave radiation (solid blue lines), and latent (solid magenta lines) and sensible (solid black lines) surface heat fluxes in 2004, 2006, and 2016 from the CFS. Longwave radiation is subtracted by 50. The dashed lines denote the climatology.

## 4. Discussion

### 4.1. SST in 2016 Breaking the Historical Record

As mentioned above, the anomalous SST rise in the second half of July and/or the first half of August, which was induced by enhanced solar radiation and weakened wind associated with a high-pressure system, resulted in the record-breaking SSTs in 2004, 2006, and 2016. During the period of the anomalous SST rise, AVHRR SST increased by 4.31°C, 4.42°C, and 3.86°C, respectively, in 2004, 2006, and 2016. The SST increase due to the high-pressure system was smaller in 2016 than in 2004 and 2006. The increase in MR OISST showed similar results. This suggests that the SST in 2016 breaking the historical record was also related to the initial SST underlying the high-pressure system. The initial AVHRR (MR) SST was 24.77°C, 24.35°C, and 25.57°C (24.67, 24.94, and 26.14°C) in these 3 years. The higher initial SST in 2016 helped the SST in 2016 breaking the historical record since satellite observations.

### 4.2. Demise of the Record-Breaking SSTs in 2004, 2006, and 2016

As shown in Figure 3, the record-breaking SST rapidly dropped in 2004 and 2006, while it initially kept at the same level and then dramatically fell in 2016. The rapid SST drop in 2004 and 2006 was induced by a strong wind event, which enhanced oceanic turbulent mixing (Figures 8 and 9). In 2016, wind enhanced slightly until a strong wind event. The slightly enhanced wind decreased SST but kept it at the same level, and then the strong wind event decreased SST dramatically. The enhancement of wind was associated with a low-pressure system migrating toward the YECS (Figures are not shown). In all these 3 years, the net surface heat flux was positive at the end of the period of the anomalous SST rise. Thus, the demise of the record-breaking SSTs was attributed to the enhancement of wind.

### 4.3. Impact of Freshwater Flux on the Record-Breaking SSTs

Strong precipitation and/or runoff may form a shallow ML by producing salt stratification above the top of the thermocline, restricting heat exchanges at the base of the ML and resulting in an anomalous SST rise (Belkin, 2009; Moon et al., 2019; Sprintall & Tomczak, 1992). During the period of the anomalous SST rise in 2004, 2006, and 2016, precipitation reduced over the YECS under the influence of the high-pressure system (Figure 12). Besides, there was no continuous heavy precipitation before the extreme SST event. Thus, precipitation over the YECS was not responsible for the shallower ML during the anomalous warming period. Changjiang diluted water showed different variations in these 3 years: It decreased in 2004 and 2006 but increased in 2016 (Figure 12). Moon et al. (2019) suggested that the increased Changjiang diluted water in 2016 spread to the area west of Jeju Island, forming a shallower ML and resulting in an anomalous SST

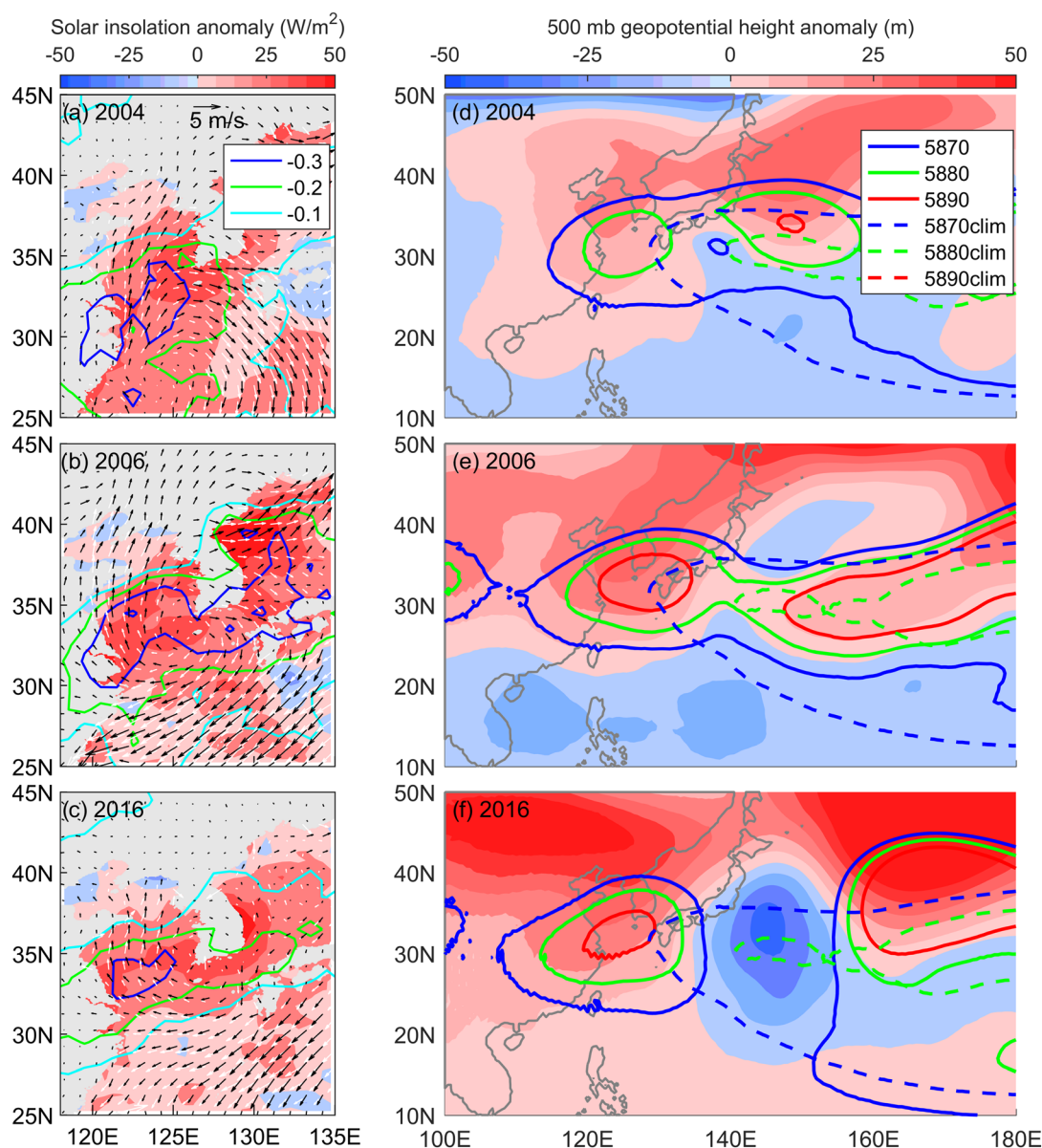


**Figure 11.** Anomalies of solar insolation (color), wind fields at the sea surface (arrow), cloud fraction (contours, a–c), and 500 mb geopotential height (color, d–f) during the period of the anomalous SST rise in 2004, 2006, and 2016. The solid and dashed contours in (d)–(f) denote 500 mb geopotential height and its climatology. The black and white arrows in (a)–(c) denote these wind field anomalies from the CFS and multisatellite blended sea winds, respectively.

warming south of 34°N (Figure 11 in Moon et al., 2019). The increased Changjiang diluted water could not entirely explain the anomalous SST rise in the YECS. In the context of the enhanced solar radiation and weakened wind over the YECS, the contribution of the increased Changjiang diluted water to the anomalous SST warming to the area west of Jeju Island needs to be further evaluated.

#### 4.4. Impact of the Kuroshio on the Record-Breaking SSTs

The Kuroshio enters the East China Sea (ECS) northeast of Taiwan then turns right and flows northeastward along the ECS shelf break toward Japan. The exchange between the Kuroshio and shelf waters plays an important role in the momentum, heat, and nutrients of the ECS (Oey et al., 2018; Wang & Oey, 2014,

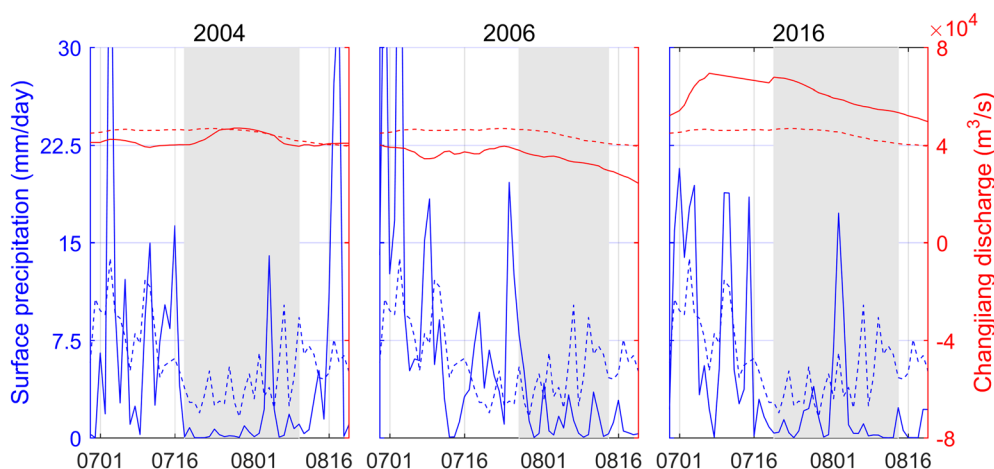


**Figure 12.** Surface precipitation (solid blue lines) and Changjiang discharge (solid red lines) in 2004, 2006, and 2016. The dashed lines denote the climatology.

2016). However, in summer, the exchange at the sea surface is limited to the shelf edge (Wang & Oey, 2016), which is most likely to have little effect on the record-breaking SSTs in the YECS. Our quantitative analysis, based on the MLT equation, also suggests that ocean advection made little contribution to the record-breaking SSTs (Figure 7).

## 5. Summary

The record-breaking SSTs in the YECS are investigated using remote sensing measurements, ocean model outputs, and atmospheric reanalysis products. Remote sensing SST shows that the YECS SST in 2004, 2006, and 2016 broke the previous record of satellite observations. Analysis results demonstrate that the record-breaking SSTs in these 3 years were mainly produced by one-dimensional vertical processes controlled by atmospheric forcing. Enhanced solar radiation and weakened wind, due to a high-pressure system over the YECS splitting from the western Pacific subtropical high, both depressed oceanic turbulent mixing, and more heat was concentrated in a shallower ML, inducing an anomalous SST rise and resulting in the record-breaking SSTs.

## Data Availability Statement

The daily optimum interpolation SST from the infrared and microwave radiometers were produced by NOAA (<https://www.ncdc.noaa.gov/oisst/data-access>) and RSS (<http://www.remss.com/measurements/sea-surface-temperature/oisst-description/>). The OFES outputs, NCEP reanalyses 1 and 2, CFS, and TRMM precipitation were downloaded from the Asia-Pacific Data-Research Center (APDRC) (<http://apdrc.soest.hawaii.edu/data/data.php>). Cloud fraction was derived from the Level-1 Atmosphere Archive and Distribution System (LAADS) Distributed Active Archive Center (DAAC) (<https://ladsweb.modaps.eosdis.nasa.gov/>). The multisatellite blended sea winds were produced by NOAA (<https://www.ncdc.noaa.gov/data-access/marineocean-data/blended-global/blended-sea-winds>).

## Acknowledgments

This study is supported by the National Key Research and Development Program of China (2016YFC1401600), Scientific Research Fund of the Second Institute of Oceanography, MNR (grants JG1909 and 14283), the National Natural Science Foundation of China (grants 41976028 and 41976003).

## References

- Banzon, V., Smith, T. M., Chin, T. M., Liu, C., & Hankins, W. (2016). A long-term record of blended satellite and in situ sea-surface temperature for climate monitoring, modeling and environmental studies. *Earth System Science Data*, 8(1), 165–176. <https://doi.org/10.5194/essd-8-165-2016>
- Bao, B., & Ren, G. (2014). Climatological characteristics and long-term change of SST over the marginal seas of China. *Continental Shelf Research*, 77, 96–106. <https://doi.org/10.1016/j.csr.2014.01.013>
- Belkin, I. (2009). Rapid warming of large marine ecosystems. *Progress in Oceanography*, 81, 207–213. <https://doi.org/10.1016/j.pocean.2009.04.011>
- Cai, R., Tan, H., & Kontoyiannis, H. (2017). Robust surface warming in offshore China Seas and its relationship to the East Asian Monsoon wind field and ocean forcing on inter-decadal timescales. *Journal of Climate*, 30, 8987–9005. <https://doi.org/10.1175/JCLI-D-16-0016.1>

- Kalnay, E., Kanamitsu, M., Kistler, R., Collins, W., Deaven, D., Gandin, L., et al. (1996). The NCEP/NCAR 40-year reanalysis project. *Bulletin of the American Meteorological Society*, 77, 437–471. [https://doi.org/10.1175/1520-0477\(1996\)077<0437:TNYRP>2.0.CO;2](https://doi.org/10.1175/1520-0477(1996)077<0437:TNYRP>2.0.CO;2)
- Kanamitsu, M., Ebisuzaki, W., Woollen, J., Yang, S. K., Hnilo, J. J., Fiorino, M., & Potter, G. L. (2002). NCEP–DOE AMIP-II reanalysis (R-2). *Bulletin of the American Meteorological Society*, 83, 1631–1644. <https://doi.org/10.1175/BAMS-83-11-1631>
- Kelly, K. A., & Qiu, B. (1995). Heat flux estimates for the western North Atlantic. Part I: Assimilation of satellite data into a mixed layer model. *Journal of Physical Oceanography*, 25(10), 2344–2360. [https://doi.org/10.1175/1520-0485\(1995\)025<2344:HFEFTW>2.0.CO;2](https://doi.org/10.1175/1520-0485(1995)025<2344:HFEFTW>2.0.CO;2)
- Kim, Y. S., Jang, C. J., Jeong, J. Y., & Shim, J. S. (2018). Daily to seasonal variability of the mixed layer depth in the central Yellow Sea: Effects of atmospheric forcing. *Journal of Coastal Research*, 85, 576–580. <https://doi.org/10.2112/SI85-116.1>
- Lee, T., Fukumori, I., & Tang, B. (2004). Temperature advection: Internal versus external processes. *Journal of Physical Oceanography*, 34(8), 1936–1944. [https://doi.org/10.1175/1520-0485\(2004\)034<1936:TAIEVP>2.0.CO;2](https://doi.org/10.1175/1520-0485(2004)034<1936:TAIEVP>2.0.CO;2)
- Lima, F., & WetHEY, D. (2012). Three decades of high-resolution coastal sea surface temperatures reveal more than warming. *Nature Communications*, 3(1), 704. <https://doi.org/10.1038/ncomms1713>
- Mann, M. E., Miller, S. K., Rahmstorf, S., Steinman, B. A., & Tingley, M. (2017). Record temperature streak bears anthropogenic fingerprint. *Geophysical Research Letters*, 44, 7936–7944. <https://doi.org/10.1002/2017GL074056>
- Mann, M. E., Rahmstorf, S., Steinman, B. A., & Miller, S. K. (2016). The likelihood of recent record warmth. *Nature Scientific Reports*, 6, 19831. <https://doi.org/10.1038/srep19831>
- Masumoto, Y., Sasaki, H., Kagimoto, T., Komori, N., Ishida, A., Sasai, Y., et al. (2004). A fifty-year eddy-resolving simulation of the world ocean—Preliminary outcomes of OFES (OGCM for the Earth Simulator). *Journal of the Earth Simulator*, 1, 35–56.
- Moisan, J. R., & Niiler, P. P. (1998). The seasonal heat budget of the North Pacific: Net heat flux and heat storage rates (1950–1990). *Journal of Physical Oceanography*, 28(3), 401–421. [https://doi.org/10.1175/1520-0485\(1998\)028<0401:TSHBOT>2.0.CO;2](https://doi.org/10.1175/1520-0485(1998)028<0401:TSHBOT>2.0.CO;2)
- Moon, J. H., Hirose, N., & Yoon, J. H. (2009). Comparison of wind and tidal contributions to seasonal circulation of the Yellow Sea. *Journal of Geophysical Research*, 114, C08016. <https://doi.org/10.1029/2009JC005314>
- Moon, J. H., Kim, T., Son, Y. B., Hong, J. S., Lee, J. H., Chang, P. H., & Kim, S. K. (2019). Contribution of low-salinity water to sea surface warming of the East China Sea in the summer of 2016. *Progress in Oceanography*, 175, 68–80. <https://doi.org/10.1016/j.pocean.2019.03.012>
- Oey, L. Y., Chang, M. C., Chang, Y. L., Lin, Y. C., & Xu, F. H. (2013). Decadal warming of coastal China Seas and coupling with winter monsoon and currents. *Geophysical Research Letters*, 40, 6288–6292. <https://doi.org/10.1002/2013GL058202>
- Oey, L.-Y., Wang, J., & Lee, M.-A. (2018). Fish catch is related to the fluctuations of a western boundary current. *Journal of Physical Oceanography*, 48(3), 705–721. <https://doi.org/10.1175/JPO-D-17-0041.1>
- Oliver, E. C. J., Donat, M. G., Burrows, M. T., Moore, P. J., Smale, D. A., Alexander, L. V., et al. (2018). Longer and more frequent marine heatwaves over the past century. *Nature Communications*, 9(1), 1324. <https://doi.org/10.1038/s41467-018-03732-9>
- Price, J. F., Weller, R. A., & Pinkel, R. (1986). Diurnal cycling: Observations and models of the upper ocean response to diurnal heating, cooling, and wind mixing. *Journal of Geophysical Research*, 106(C4), 6943–6955. <https://doi.org/10.1029/2000JC000479>
- Qu, T. (2001). Role of ocean dynamics in determining the mean seasonal cycle of the South China Sea surface temperature. *Journal of Geophysical Research*, 106(C4), 6943–6955. <https://doi.org/10.1029/2000JC000479>
- Reynolds, R. W., Smith, T. M., Liu, C., Chelton, D. B., Casey, K. S., & Schlax, M. G. (2007). Daily high-resolution-blended analyses for sea surface temperature. *Journal of Climate*, 20(22), 5473–5496. <https://doi.org/10.1175/JCLI-D-14-00293.1>
- Rosati, A., & Miyakoda, K. (1988). A general circulation model for upper ocean simulation. *Journal of Physical Oceanography*, 18(11), 1601–1626. [https://doi.org/10.1175/1520-0485\(1988\)018<1601:AGCMFU>2.0.CO;2](https://doi.org/10.1175/1520-0485(1988)018<1601:AGCMFU>2.0.CO;2)
- Saha, S., Moorthi, S., Pan, H. L., Wu, X., Wang, J., Nadiga, S., et al. (2010). The NCEP climate forecast system reanalysis. *Bulletin of the American Meteorological Society*, 91, 1015–1058. <https://doi.org/10.1175/2010BAMS3001.1>
- Saha, S., Moorthi, S., Wu, X., Wang, J., Nadiga, S., Tripp, P., et al. (2014). The NCEP climate forecast system version 2. *Journal of Climate*, 27, 2185–2208. <https://doi.org/10.1175/JCLI-D-12-00823.1>
- Sasaki, H., Nonaka, M., Masumoto, Y., Sasai, Y., Uehara, H., & Sakuma, H. (2008). An eddy-resolving hindcast simulation of the quasi-global ocean from 1950 to 2003 on the Earth Simulator. In K. Hamilton, & W. Ohfuchi (Eds.), Chapter 10 *High Resolution Numerical Modelling of the Atmosphere and Ocean* (pp. 157–185). New York: Springer. [https://doi.org/10.1007/978-0-387-49791-4\\_10](https://doi.org/10.1007/978-0-387-49791-4_10)
- Smale, D. A., Wernberg, T., Oliver, E. C. J., Thomsen, M., Harvey, B. P., Straub, S. C., et al. (2019). Marine heatwaves threaten global biodiversity and the provision of ecosystem services. *Nature Climate Change*, 9, 306–312. <http://doi.org/10.1038/s41558-019-0412-1>
- Sprintall, J., & Tomczak, M. (1992). Evidence of the barrier layer in the surface-layer of the tropics. *Journal of Geophysical Research*, 97(C5), 7305–7316. <https://doi.org/10.1029/92JC00407>
- Tan, H., & Cai, R. (2018). What caused the record-breaking warming in East China Seas during August 2016? *Atmospheric Science Letters*, 19(10), e853. <https://doi.org/10.1002/asl.853>
- Wang, J., & Oey, L.-Y. (2014). Inter-annual and decadal fluctuations of the Kuroshio in East China Sea and connection with surface fluxes of momentum and heat. *Geophysical Research Letters*, 41, 8538–8546. <https://doi.org/10.1002/2014GL062118>
- Wang, J., & Oey, L.-Y. (2016). Seasonal exchanges of Kuroshio and shelf waters and their impacts on the shelf currents of the East China Sea. *Journal of Physical Oceanography*, 46(5), 1615–1632. <https://doi.org/10.1175/JPO-D-15-0183.1>
- Wu, R., Li, C., & Lin, J. (2017). Enhanced winter warming in the eastern China coastal waters and its relationship with ENSO. *Atmospheric Science Letters*, 18(1), 11–18. <https://doi.org/10.1002/asl.718>
- Xia, C., Qiao, F., Yang, Y., Ma, J., & Yuan, Y. (2006). Three-dimensional structure of the summertime circulation in the Yellow Sea from a wave-tide-circulation coupled model. *Journal of Geophysical Research*, 111, C11S03. <https://doi.org/10.1029/2005jc003218>
- Zhang, H.-M., Reynolds, R. W., & Bates, J. G. (2006). *Blended and gridded high resolution global sea surface wind speed and climatology from multiple satellites: 1987–present*. Atlanta, CA: Proceedings of the 86th AMS Annual Meeting.